Journal of Materials Chemistry C

REVIEW

Cite this: *J. Mater. Chem. C*, 2025, **13**, 4876

Structural design and controlled fabrication of advanced airflow sensors

Qinyuan Jiang, Khaixien Leu, Fei Wang, Run Li, Kangkang Wang, Yanlong Zhao, Aike Xi, Yonglu Zang and Rufan Zhang *

Received 5th December 2024,
Accepted 7th February 2025

DOI: 10.1039/d4tc05127k

rsc.li/materials-c

Airflow sensors are in huge demand in many fields such as the aerospace industry, weather forecasting, environmental monitoring, chemical and biological engineering, health monitoring, wearable smart devices, *etc.* Faced with the growing need in intelligent and integrated applications, airflow sensors with higher performance, improved compatibility and multiple functions have attracted wide attention in the fields of sensing, mechanics, and nanotechnology, while the great challenges in structural design and controlled fabrication still remain. So far, researchers have developed various strategies and techniques in the aspects of functional materials, device configurations, and integrated systems, enabling more advanced applications for airflow sensors. In this review, we first introduce the basic working mechanisms of airflow sensors, followed by the proceedings in functional materials and device configurations. The progress in the system integration of airflow sensors is also summarized to demonstrate their compatibility with other functional devices, which leads to their great potential in various application demonstrations. Finally, the possible directions for optimizing airflow sensing performance and broadening application scenarios are listed.

1. Introduction

This era of information and intelligence technologies has witnessed the rapid development of smart manufacturing, fifth generation (5G) of mobile communication, Internet of Things (IoT), robotics, advanced healthcare, *etc.*, in which high-performance sensors which have intelligence, multiple functions, and high degree of integration are in huge demand.[1–5] Sensors are the fundamental devices that can transduce external stimuli into measurable signals (usually electrical signals). In the cases of airflow sensors, they are designed to quantitatively capture the information carried by airflows, including

Beijing Key Laboratory of Green Chemical Reaction Engineering and Technology, Department of Chemical Engineering, Tsinghua University, Beijing 100084, China. E-mail: zhangrufan@tsinghua.edu.cn

Qinyuan Jiang

Dr Qinyuan Jiang received his bachelor's degree in Chemical Engineering and Technology from the East China University of Science and Technology in 2019 and his PhD degree in Chemical Engineering and Technology from Tsinghua University in 2024. His research focuses on the controlled synthesis, properties, and applications of ultralong carbon nanotubes.

Rufan Zhang

Prof. Rufan Zhang received his bachelor's degree in Chemical Engineering and Technology from the China University of Petroleum (Beijing) in 2009 and his PhD degree in Chemical Engineering and Technology from Tsinghua University in 2014. From 2014 to 2017, he worked as a postdoctoral researcher in the Department of Materials Science and Engineering at Stanford University. Now Prof. Zhang is an associate professor in the Department of Chemical Engineering, Tsinghua University. His research interests include the controlled synthesis and property study of carbon nanotubes, photothermal regulation materials, advanced electrocatalysts, etc.

speed, direction, and flow rate (the integral of speed on a specific cross section).[6,7] Airflow sensors are playing key roles in fields such as aerospace, environmental monitoring, chemical and biological engineering, health monitoring, wearable smart devices, *etc.*[8–14] and are facilitating the development of human society towards higher degrees of automation, integration, and intelligence.

Since the invention of early models such as Pitot and Venturi tubes,[15,16] researchers have been pursuing better solutions for achieving higher airflow sensing performance (higher sensitivity, shorter response time, lower detection threshold, lower zero drift, wider detection range, higher durability, *etc.*), extended functions, a higher degree of integration, and higher compatibility with various working scenarios.[17,18] Correspondingly, novel working mechanisms, involving the interplay of multiple physical fields and the unconventional properties of functional materials, have been extensively proposed to boost the development of airflow sensors.[19] Compared with the pressure drop–velocity relationship used in traditional Pitot and Venturi tubes, the enriched working mechanisms offer more opportunities for transducing other physical signals and catalyzing the applications in more fields. Based on these working mechanisms, researchers also endeavored to design elaborate functional materials and device configurations to further improve the airflow sensing performance. For instance, many works on piezoresistive airflow sensors constructed hierarchical composites consisting of macroscale flexible matrices and nanoscale conductive networks, which provided much room for the optimization of sensing performance.[20,21] Furthermore, with the growing demand in multifunctional sensors, as well as the great advances in micro- and nano-manufacturing, integrated sensing systems consisting of miniaturized airflow sensors are becoming more and more popular due to their improved sensing performance and extended functionalities.[22] Finally, new applications of advanced airflow sensors are also blooming with the assistance of the above concepts and techniques, offering revolutionary opportunities to the fields of industrial production, human health, environmental ecology, *etc.*[23]

Although many advancements have been reported, the design and fabrication of airflow sensors are still far from mature, which in turn hinders their further applications in industrial products. Since the reviews on specific types of airflow sensors or specific application areas have been reported elsewhere,[19,24,25] this review mainly aims to give a vision of the general principles of airflow sensors, summarize the latest proceedings related to their structural design and controlled fabrication, and provide perspectives on the challenges and opportunities.

The overview of this review is shown in Fig. 1. We first introduce the basic working mechanisms of several airflow sensors, including thermal, piezoresistive, piezoelectric, triboelectric, and optical effects. Then, we thoroughly discuss the functional materials and device configurations in the state-of-the-art airflow sensors to interpret their structural designs, fabrication processes, and resultant performances. Moreover, the integrated sensing systems consisting of advanced airflow sensors and other sensors are also introduced to gain insights into their design concepts and broadened functions. Based on the above proceedings in design and fabrication, the application demonstrations presented in latest works are summarized, including respiratory monitoring, flow rate measurement, and motion and environment perception. Finally, we conclude the challenges and propose several perspectives on the material selection and synthesis, device design, and system integration of advanced airflow sensors.

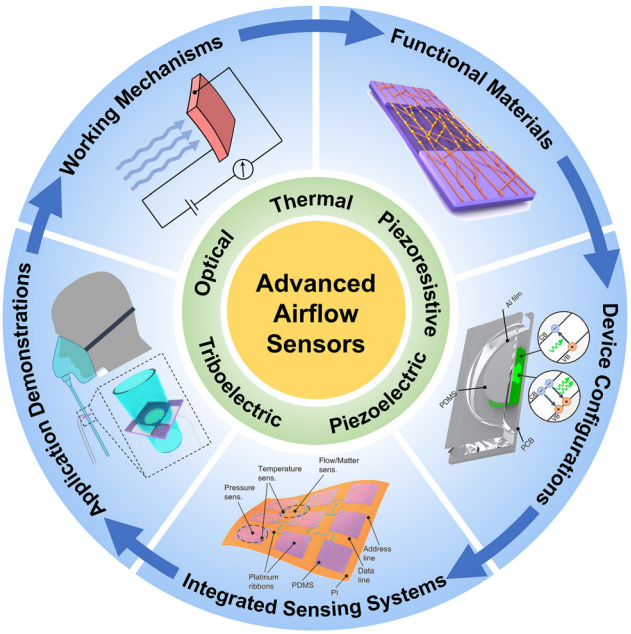

Fig. 1 Overview of the structural design and controlled fabrication of airflow sensors. Figures are adapted from ref. 26, Wiley-VCH 2022; ref. 27, Springer Nature 2022; ref. 11, Wiley-VCH 2023; and ref. 28, American Chemical Society 2024.

2. Working mechanisms of airflow sensors

Before introducing the proceedings in the structural design and controlled fabrication, we first review the typical working mechanisms of various airflow sensors, including thermal, piezoresistive, piezoelectric, triboelectric, and optical effects, so as to lay the foundation for the following part of sensors' design and fabrication.

2.1. Thermal effects

Thermal airflow sensors are generally based on the heat exchange between sensors and airflows and the electrical responses stemming from the temperature-dependent resistances of functional materials.[29] In a typical thermal airflow sensor, the temperature of an electrically conductive material is elevated by applying a constant direct current (DC) due to the Joule heating effect, while the generated heat is then balanced by the convective heat dissipation in airflow with a certain velocity (Fig. 2a).[30] Metals and carbon materials are usually

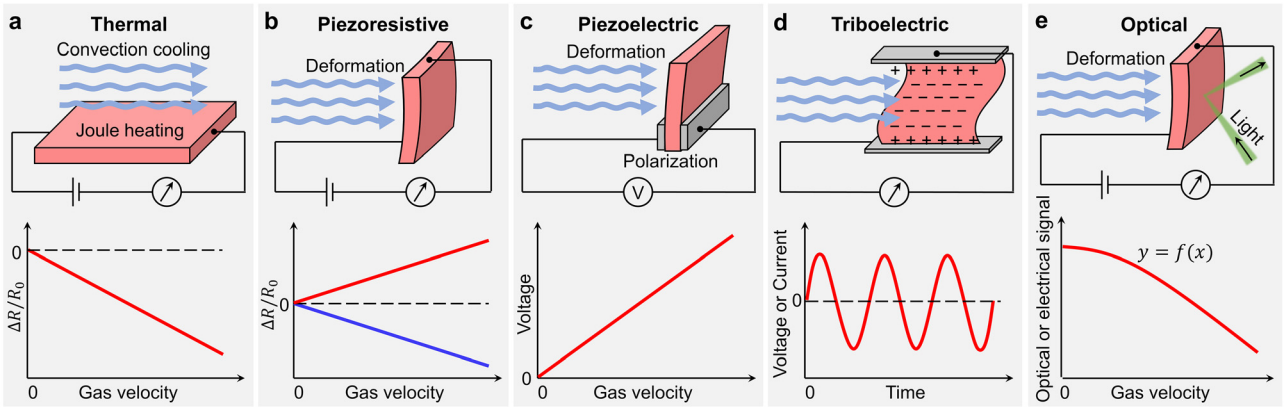

Fig. 2 Working mechanisms of airflow sensors. Structures and typical outputs of (a) thermal, (b) piezoresistive, (c) piezoelectric, (d) triboelectric, and (e) optical airflow sensors.

used as functional materials due to their high electrical and thermal conductivities, good processing feasibilities, and well-established physical properties.[31–33] As shown in the lower panel of Fig. 2a, the relative resistance variation ($\Delta R/R_0$) is negative in most cases because the resistance of a metallic material decreases when it is cooled.[29] According to the temperature–resistance relationship of a specific material, the heat transfer coefficient can be determined by reading the resistance, and the gas velocity can thus be derived due to its direct correlation with the heat transfer coefficient.

According to the geometries of functional materials, thermal airflow sensors can be further categorized into hot-wire and hot-film sensors. Hot-wire sensors are endowed with high sensitivity due to the all-round contact between wires and the surrounding airflows, while they also suffer from the mechanical fragility of thin wires.[34] In contrast, hot-film sensors usually possess high flexibility, small disturbance to flow fields, and remarkable compatibility with curved surfaces, which significantly broaden their application scenarios.[35]

2.2. Piezoresistive effects

Piezoresistive airflow sensors are a family of sensors with simple device structures and facile signal acquisitions. The functioning of piezoresistive airflow sensors relies on the resistance variations caused by airflow-induced deformations (Fig. 2b).[36] The specific reason for resistance variations may varies for different material systems. In the simplest case, the existence of strains in a pure material will induce the shifts in band structures as well as their filling states, which will in turn alter the electrical resistivity.[37] Both pure metals and semiconductors can serve as the functional parts of piezoresistive airflow sensors, in which the piezoresistive effects of semiconductors (*e.g.*, silicon) are usually more prominent.[36,38]

As for the cases of composites, which can be seen as the combination of conducting networks and flexible matrices, the origin of the piezoresistive effect is much more complicated. Firstly, similar to pure materials, conducting materials within the composites may exhibit their own piezoresistive behaviors. Besides, in the presence of deformations, the connectivity of conducting networks may undergo drastic changes, leading to the variations in the total resistance.[20,39,40] Even without noticeable changes in the network connectivity, the junction resistance between two conducting materials may not remain constant due to interfacial interactions.[26] Considering the complex electromechanical behaviors in composite systems, the electrical output ($\Delta R/R_0$) of a piezoresistive airflow sensor may present either positive or negative dependence on gas velocity (Fig. 2b),[26,41] which brings more intriguing opportunities for the structural design and performance optimization.

2.3. Piezoelectric effects

The ability to generate polarization voltages when applied with external stresses, *i.e.*, piezoelectric effects, originates from the broken inversion symmetry of a crystal material.[42] In typical piezoelectric sensors, airflow-induced deformations in piezoelectric materials will cause the shifts of positive and negative charges' centers, thus forming a detectable voltage between two electrodes (Fig. 2c).[43] With higher gas velocities and larger deformations, polarization voltages are accordingly larger, which indicates a direct electromechanical transformation capability and lays a solid foundation for the quantitative sensing. Moreover, no extra power supply is needed in the cases of piezoelectric airflow sensors, which demonstrates their potential in realizing self-powered devices or even self-powered integrated sensing systems if combined with energy conversion and storage devices.[44]

So far, piezoelectric materials such as ceramics ($BaTiO_3$, $PbZr_{0.52}Ti_{0.48}O_3$, *etc.*) and crystalline polymers (polyvinylidene difluoride (PVDF), poly(vinylidene-trifluoroethylene) (P(VDF-TrFE)), *etc.*) have been extensively reported to facilitate airflow sensing.[42,45,46] As for the criteria of suitable materials in piezoelectric sensors, both the piezoelectric voltage coefficient and flexibility should be taken into consideration to meet the complex working conditions in real applications.[47] In the aspect of device configurations, much effort has been made in the optimization of sensor geometries to maximize strains and the resultant piezoelectric effects, in which fiber-shaped sensors are ideal candidates for sensitively perceiving airflows

due to their high flexibility and great potential in directional sensing.[45,46]

2.4. Triboelectric effects

Triboelectric nanogenerators (TENGs) represent a group of devices that convert the energy in the surrounding environment into electricity through frictions, based on the coupling effect of contact electrification and electrostatic induction.[19] As shown in Fig. 2d, a typical triboelectric airflow sensor consists of a piece of flexible film (polymer films in most cases) and two fixed metal electrodes, of which the configuration is similar to parallel plate capacitors.[48] When a stream of airflow is introduced between the two electrodes, the flexible film vibrates at a certain frequency and periodically rubs the electrodes, leaving non-zero net charges on both surfaces and thus generating periodic voltages. By measuring the real-time voltage (or current) signals and extracting their frequencies and amplitudes, a quantitative relationship between electric signals and gas velocities can be established.[49] Similar to the piezoelectric effect, the triboelectric effect also enables self-powered airflow sensors,[13] while fast Fourier transform (FFT) is usually necessary to analyze the frequencies and amplitudes of periodic signals, which brings additional complexities to device structures.

An ideal triboelectric material used in airflow sensors should possess not only a distinct electron affinity from that of electrodes, but also sufficient flexibility and lightweight so as to facilitate the periodic frictions when applied with gentle airflows.[49] Moreover, many novel device configurations and operation modes of triboelectric sensors have also been reported, such as contact-separation, linear-sliding, single-electrode, and freestanding triboelectric-layer modes,[50] which further improved the sensing performance and broadened application scenarios.

2.5. Optical effects

Optical effects can also be utilized to perceive airflows with delicate structural designs, and the corresponding sensors are referred as optical airflow sensors.[51,52] As shown in Fig. 2e, the airflow-induced deformations may change the optical properties of pure materials or their composites, causing the variations in absorption, reflection, or transmission spectra, which can be directly collected using spectrometers or converted into electric signals using photodetectors.[53] Moreover, light sources (*e.g.*, lasers) are usually needed to be included in optical airflow sensors to guarantee a constant wavelength and intensity of the incident light.[27] Therefore, the outputs of optical airflow sensors can be more complicated than others, and the specific optical signal–velocity (or electrical signal–velocity) relationships strongly depend on material properties and device configurations. Due to the advantages of fast optical responses, high sensitivity, lightweight, miniaturized devices, *etc.*, optical airflow sensors are receiving growing research interest and seeding more novel working principles and advanced device structures.

3. Design, fabrication, and application of airflow sensors

3.1. Functional materials and device configurations

The performance metrics of airflow sensors (*e.g.*, sensitivity, detection range, response time, durability, *etc.*) are simultaneously determined by the choices of functional materials, the designs of device configurations, and the fabrication processes. Faced with the growing demands in constructing integrated sensing systems and achieving various application purposes, high-performance airflow sensors with delicate designs and controlled fabrication processes have become the focus in this field. In this part, we systematically introduce the proceedings in the advanced designs of thermal, piezoresistive, piezoelectric, triboelectric, and optical airflow sensors, and give brief interpretations of their outstanding sensing performance.

3.1.1. Thermal airflow sensors. As introduced in the working mechanism section, thermal airflow sensors, which usually include hot-wire and hot-film sensors, transduce temperature variations into electrical signals, in which the functional materials and device geometries strongly affect the device performance.[54] For example, when the temperature drop remains constant, a higher temperature coefficient of resistivity (TCR) of the functional material will cause a larger resistance variation, which indicates improved sensitivity.[24] As for the influence of device geometries, for instance, the length-to-diameter ratio of a hot-wire sensor significantly affects the heat conduction behavior at the connections, which will induce the non-ideal deviations in temperature and resistance.[32]

In recent years, miniaturized thermal airflow sensors based on microelectromechanical systems (MEMS) have attracted wide attention due to reduced power consumption, higher sensitivity, less disturbance with airflows, and the feasibility of incorporation into complex sensing systems.[24,55] For instance, Talbi *et al.* designed and fabricated microscale hot-wire sensors consisting of low stress Ni/W multilayers and a nanocrystalline diamond (NCD) layer (Fig. 3a).[32] Ni/W multilayers endowed this hot-wire sensor with a high TCR (1700 ppm K^{-1}) and thus high sensitivity, as well as a very low residue stress (<200 MPa), which would be beneficial for improving the robustness. Moreover, the NCD layer with high mechanical toughness provided a strong support for the wire, and its low thermal conductivity (<10 W m^{-1} K^{-1}) enabled a good thermal insulation and thus reduced the conductive end losses. As a result, sub-millimetric hot-wire sensors realized the unobtrusive sensing in the range of 0.5–30 m s^{-1} with high reliability and robustness. In order to make sensors compatible with integrated circuits (ICs), Najafi *et al.* proposed the design of hair-like hot-wire sensors.[34] Hair-like hot-wire sensors were easily fabricated with standard wire bonders used in the post-process steps of ICs and could be arranged into various sensor arrays with different shapes and materials (Fig. 3b). Both Al and Pt wires were utilized to fabricate the sensors, resulting in wide detection range (0.01–17.5 m s^{-1}) and high accuracy (0.06% for Pt wires in the low-speed regime and 2.5% for Al wires in the high-speed regime).

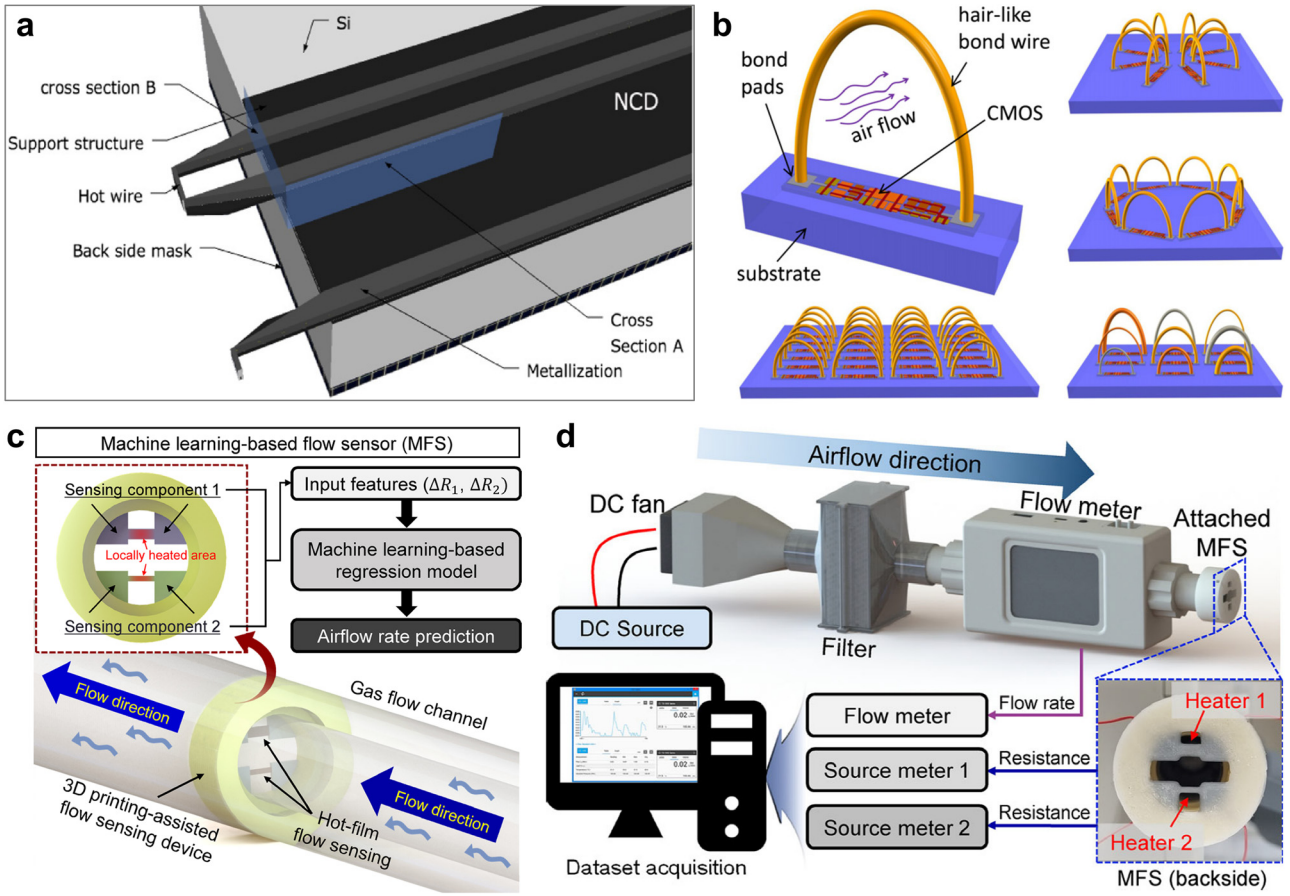

Fig. 3 Advanced thermal airflow sensors. (a) Schematic illustration of a microscale hot-wire sensor. Reproduced with permission from ref. 32. Copyright 2015, IOP Publishing. (b) Schematic illustrations of hair-like hot-wire sensors and ICs with different arrangements. Reproduced with permission from ref. 34. Copyright 2013, IOP Publishing. (c) Schematic illustration of a hot-film sensor based on machine learning and (d) the experimental setup for measuring datasets. Reproduced with permission from ref. 29. Copyright 2024, Wiley-VCH.

As for hot-film sensors, there are also many emerging designs with extended functions and excellent performance. For example, Norford *et al.* embedded three MEMS hot-film sensors into a cylinder-shaped probe (6 mm in diameter) to realize the simultaneous detection of speed and direction.[31] The MEMS hot-film sensors were constructed by sputtering Ti/Pt films (10/100 nm), which were then patterned by a standard lift-off process. Three sensors were arranged in three directions with an angle of 120°, *i.e.*, forming a cylindrical anemometer, for collecting the gas velocities from different directions. Therefore, high speed accuracy (3.6% in the range of 1–10 m s^{-1}) and angle accuracy (1.2° in the range of 0–360°) were achieved, demonstrating their great potential in the miniaturization of practical devices. In addition to the innovations in materials and device configurations, accessory techniques were also developed to assist the application of thermal airflow sensors. So *et al.* utilized machine learning (ML) techniques to interpret the signals from hot-film sensors and compared the performance of three ML multivariate regression models, *i.e.*, multiple linear regression (MLR), *k*-nearest neighbor (KNN), and deep neural network (DNN) models.[29] As shown in the workflow and experimental setup (Fig. 3d and e), 8400 experimental data collected using two sensing components were used for the training of MLR, KNN, and DNN models, and their performances were then evaluated by comparing the accuracies of prediction. They found that the mean absolute error and mean squared error of the KNN model obtained by tensor fusion techniques could be as low as 0.01522 and 0.00132, respectively, which provided an effective tool for managing airflow sensor systems.

Although the basic configurations of thermal airflow sensors are well established, more and more advanced concepts and devices are still being proposed. Owing to the miniaturized sizes, structural stability (without moving parts), and remarkable performance (high sensitivity, fast response, wide detection range, *etc.*), thermal airflow sensors are expected to be the ideal building blocks of advanced sensing systems.

3.1.2. Piezoresistive airflow sensors. With the rapid development of nanotechnologies, utilizing nanomaterials and their composites to construct piezoresistive airflow sensors has become an effective way to achieve excellent device performance and diverse functions. High flexibility and light weight

are generally the prerequisites for an ideal functional material in piezoresistive sensors because they are favorable for swiftly generating sufficient deformations in airflows so as to induce resistance variations.[40] Hence, the potential of nanowires, carbon nanomaterials (carbon nanotubes (CNTs), graphene, *etc.*), and polymers has been extensively explored, leading to the emergence of various high-performance piezoresistive airflow sensors with different configurations.[21,38,56–61]

The first category of piezoresistive airflow sensors based on pure piezoresistive materials is noted for their structural simplicity and clear structure–performance relationship. For example, inspired by animals' sensing of subtle airflows with their hair cells, Zhang *et al.* fabricated biomimetic hair sensors based on Si nanowires (SiNW-BHSs) and successfully constructed flexible sensor arrays to perceive airflows on curved surfaces (Fig. 4a).[38] The high aspect ratio (~1000) of SiNWs provided an outstanding flexibility, which rendered SiNWs

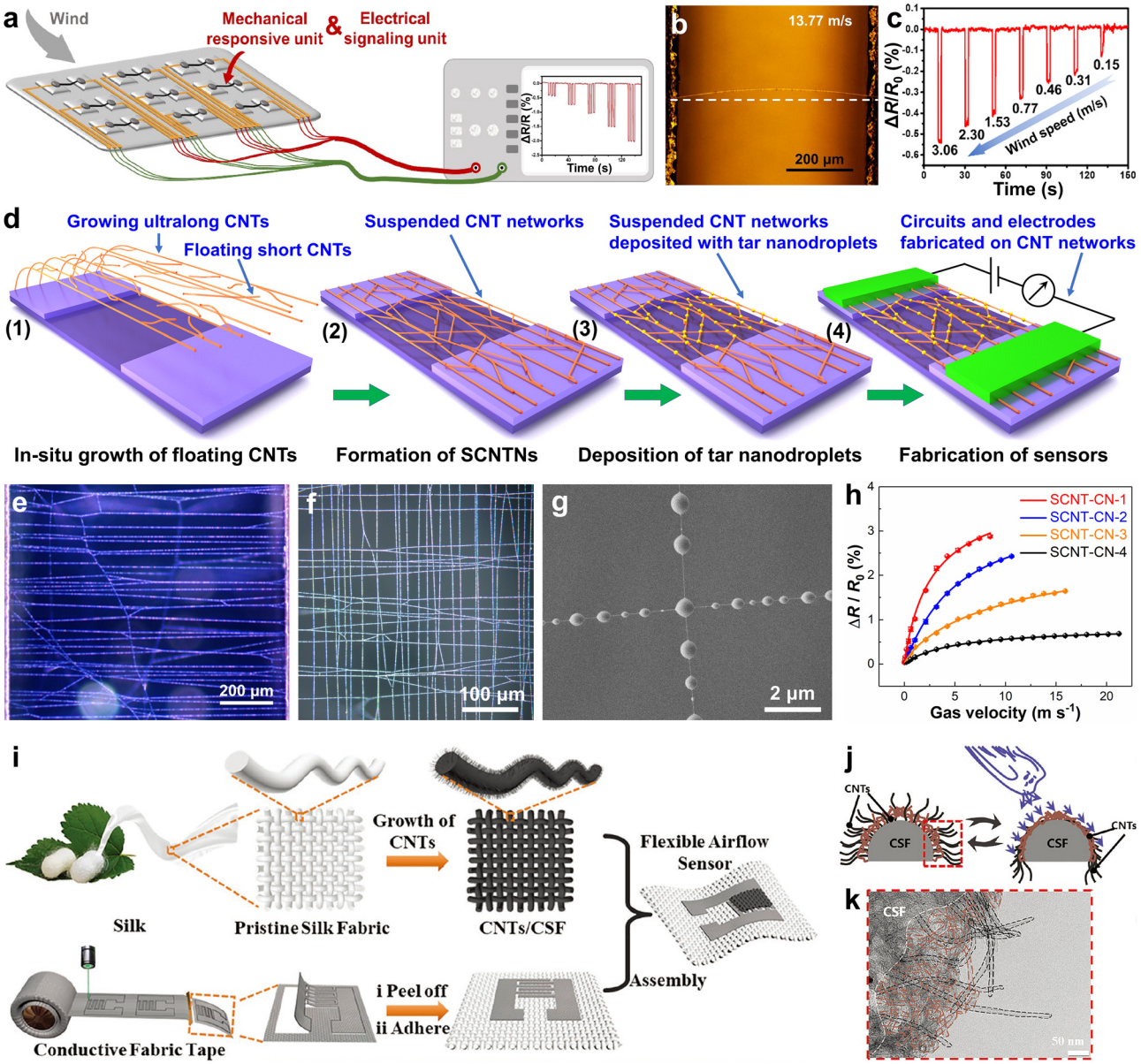

Fig. 4 Advanced piezoresistive airflow sensors. (a) Schematic illustration of a SiNW-BHS sensing array. (b) Optical microscopy image of SiNW hairs with airflow loadings. (c) Relationship between the relative resistance variation and the wind speed. Reproduced with permission from ref. 38. Copyright 2021, American Chemical Society. (d) Schematic illustration of the synthesis process and (e) optical microscopy image of SCNTN-based airflow sensors. Reproduced with permission from ref. 26. Copyright 2022, Wiley-VCH. (f) Optical microscopy image, (g) SEM image, and (h) relative resistance variation–gas velocity relationships of SCNT-CN-based airflow sensors. Reproduced with permission from ref. 28. Copyright 2024, American Chemical Society. (i) Schematic illustration of the fabrication procedures of CNTs/CSF. (j) Schematic illustration of the structural changes of CNTs/CSF in response to airflows. (k) Transmission electron microscopy (TEM) image of the extended CNTs and curved CNTs on the surface of CSF. Reproduced with permission from ref. 41. Copyright 2020, Wiley-VCH.

being easy to deform in airflows and thus generate piezoresistive signals (Fig. 4b). Consequently, SiNW-BHSs exhibited compact device structures, a low detection limit (< 0.15 m s^{-1}, Fig. 4c) and a short response time (< 40 ms).

In addition to the direct acquisition of piezoresistive signals in pure materials, the dynamic junction resistances in conductive networks can also invoke similar responses. In recent years, our group developed a substrate interception and direction strategy (SIDS) to grow ultralong CNTs with ultrahigh yields, which in turn facilitated the controlled synthesis of suspended CNT networks (SCNTNs).[26,62,63] As shown in Fig. 4d and e, with the assistance of van der Waals interactions, ultralong CNTs over a trench on the substrate will self-assemble into network structures, which perfectly inherited the intrinsic extraordinary properties of CNTs, including high flexibility, light weight, and high conductivity. After optically visualized by tar nanodroplets and deposited with metal contacts,[64] SCNTNs were fabricated into ultrasensitive airflow sensors with a short response time of 0.021 s, a high sensitivity of 0.0124 s m^{-1} and a small detection threshold of 0.11 m s^{-1}. Interestingly, the variations in CNTs' resistances were found to be trivial in sensing tests, implying the critical role of junction resistances. By testing the acoustic responses and establishing a forced vibration model, the piezoresistive responses were confirmed to be strongly correlated with the intertube stress at X junctions, *i.e.*, the sensing behaviors were based on the dynamic junction resistances in conductive networks. Afterwards, we further proposed the design of suspended ultralong CNT crossed networks (SCNTCNs) to increase the mechanical robustness while retaining a high sensitivity by increasing the proportion of X junctions.[28] Highly ordered network structures with abundant X junctions and tunable areal densities were obtained by a two-step growth method in perpendicular directions (Fig. 4f and g), resulting in a significantly widened detection range of 0.02–21.22 m s^{-1} and improved the overall sensing performance and practicality.

Inducing a dynamic connectivity in a conducting matrix under external stimuli is also an explicit way for realizing piezoresistive airflow sensing, especially for composite systems. These composites usually consist of at least two components with distinct conductivities, in which the component with higher conductivity plays a critical role because it serves as the building block of conducting pathways.[65,66] So far, many researchers have proposed effective strategies for combining conductive components with certain substrates and optimizing the airflow sensing performance. For instance, Zhang *et al.* reported the *in situ* growth of fluff-like CNTs on carbonized silk fabric (CSF), forming all-textile CNTs/CSF airflow sensors (Fig. 4i).[41] Owing to the flexibility of CNTs/CSF and interdigitated electrodes (commercial nickel-coated fabric), CNTs/CSF-based sensors could be attached to fabric surfaces, which would be beneficial for the development of wearable electronics. Moreover, CNTs/CSF-based airflow sensors possessed outstanding sensing performance, such as an ultralow detection limit ($\sim$0.05 m s^{-1}), a multiangle airflow differential response (0°–90°), a fast response time ($\sim$1.3 s), and a wide detection range (0.05–7.0 m s^{-1}). To interpret the sensing mechanism of CNTs/CSF, the authors proposed the electromechanical model shown in Fig. 4j. When airflows were introduced, the resistance of the CSF barely changed, while the foam-like layer consisting of curved CNTs (marked with brown color) and extended CNTs (marked with black color) became more compact (Fig. 4k). With the increase of junction points, the resistance of this foam-like layer could be drastically reduced, *i.e.*, forming a highly conductive layer wrapping the CSF, which induced a negative piezoresistive effect in CNTs/CSF-based airflow sensors.

The novel designs of functional materials and device configurations have given rise to the booming development of piezoresistive airflow sensors. With the assistance of interdisciplinary studies, including physics, chemistry, materials science, *etc.*, piezoresistive airflow sensors are expected to exhibit higher sensing performance, mature fabrication processes, and higher compatibility with downstream applications.

3.1.3. Piezoelectric airflow sensors. Piezoelectric airflow sensors can transform deformations (mechanical energy) into voltage signals (electric energy) due to the electromechanical nature of their functional parts, providing abundant opportunities for fabricating self-powered devices with simple structures. So far, several proceedings have proven that both material selections and device designs contribute to the improvement in the overall performance of piezoelectric airflow sensors.[45–47]

Among various piezoelectric materials, polymers (*e.g.*, PVDF and P(VDF-TrFE)) are usually considered as ideal candidates for airflow sensing applications due to their notable flexibility under large deformations, in contrast to the brittleness of piezoelectric ceramics.[46] These polymers are generally combined with flexible substrates or electrodes with cantilever- or film-like geometries to maximize their deformations in airflow sensing.[67,68] For example, Zhao *et al.* developed the piezoelectric airflow sensors based on PVDF cantilevers to simultaneously measure the airflow direction and speed (Fig. 5a and b).[69] With the assistance of specially designed groove array frames, PVDF cantilevers covered with Cu foils could vibrate in airflows with larger amplitudes, which then resulted in stronger piezoelectric responses. Through establishing a fluid-solid-electric coupling model based on finite element methods (FEMs), a larger pressure gradient was observed in the case of groove array frames, which facilitated the generation of vigorous vibrations. As a result, this PVDF cantilever-based airflow sensor exhibited significant responses to airflows with different directions and velocities, and a parabolic relationship between the output voltage and the gas velocity was observed (Fig. 5c). In addition to cantilever-like configurations, film-like structures are also commonly used for piezoelectric airflow sensors due to their robustness, processability, and compatibility with curved surfaces. A piezoelectric sensing film (PSF) was proposed by Duan *et al.* consisting of a flexible substrate with preset interdigitated electrodes (IDEs) as well as electrospun P(VDF-TrFE) fibers (Fig. 5d).[68] This PSF airflow sensor could be settled in a flow field to perceive the normal pressure differences between two sides, and then transduce deformations into voltage signals. Due to the non-uniform strains in the longitudinal

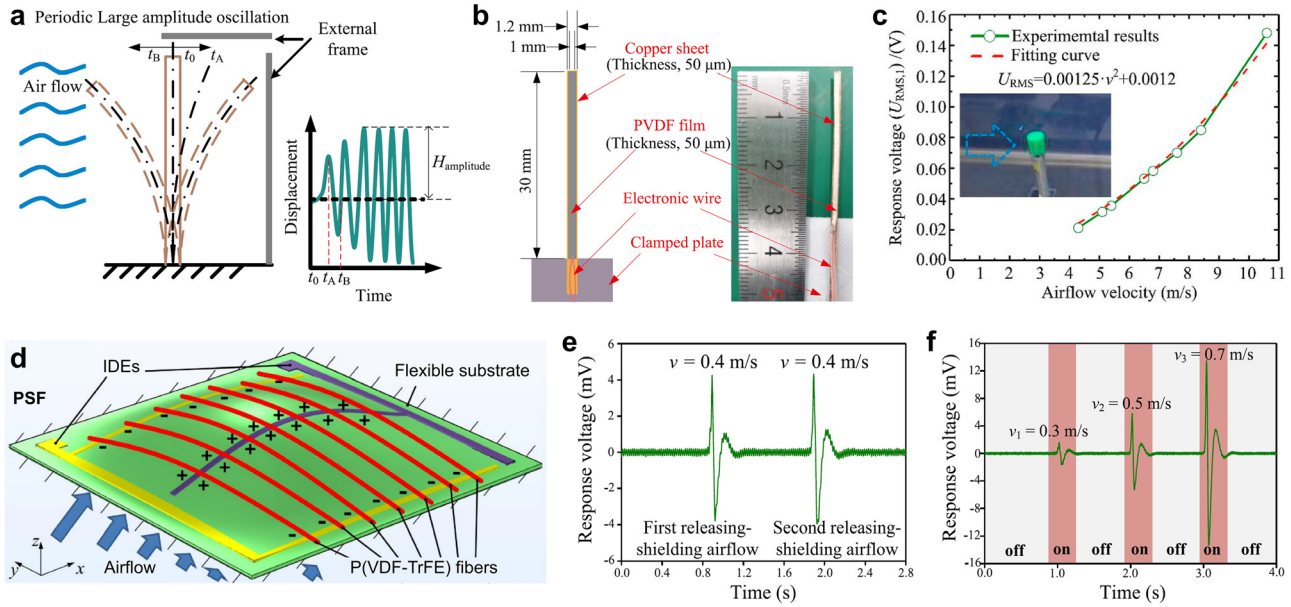

Fig. 5 Advanced piezoelectric airflow sensors. (a) Schematic illustration of the vibration sensing realized using a PVDF cantilever. (b) Schematic illustration and photograph of a PVDF cantilever-based piezoelectric sensor. (c) Response characteristics of a PVDF cantilever-based piezoelectric sensor. Reproduced with permission from ref. 69. Copyright 2019, Elsevier. (d) Schematic illustration of the electromechanical behavior of P(VDF-TrFE) fiber-based piezoelectric sensors. (e) and (f) Typical dynamic responses of P(VDF-TrFE) fiber-based piezoelectric sensors. Reproduced with permission from ref. 68. Copyright 2022, Elsevier.

direction of P(VDF-TrFE) fibers, positive and negative charges accumulated at the center and edges of the PSF, respectively, were then collected by IDEs. Based on the above rational designs of PSFs, a low detection limit of 0.3 m s^{-1}, a high sensitivity of 15 mV m^{-1} s, and a fast response behavior (30 ms and 200 ms for the response time and recover time, respectively) were achieved (Fig. 5e and f). Moreover, the output characteristics were highly consistent with numerically derived results, demonstrating the well-defined physical model of PSF airflow sensors.

The past decades have witnessed the remarkable development of novel piezoelectric airflow sensors, while tremendous challenges still remain. Many piezoelectric airflow sensors rely on the vibrational movements of their functional parts to generate measurable signals. However, the reading, processing and translating of these oscillating electrical signals with varying signal-to-noise ratios are challenging, particularly for miniaturized devices. Besides, as the output of a piezoelectric airflow sensor heavily depends on the gas velocity and is usually unstable, the construction of self-powered sensing systems may require the incorporation of energy storage devices, which will further complicate the structural designs and fabrication processes.

3.1.4. Triboelectric airflow sensors. Since the first report of TENGs by Wang *et al.*,[70] triboelectric effects have been widely employed in the sensing of various fluids, including both liquid and gas, based on the flapping motions of moving parts propelled by fluids and the resultant triboelectrification and electrostatic induction behaviors. Mechanical energy scavenging and self-powered devices can also be realized *via* triboelectric flow sensors. In this context, many sensor configurations have been developed to utilize the kinetic energy of airflows and maximize electrical signals.[13,71–77] In previous reports, a flexible and freestanding polymer film with a strong electron affinity (usually fluorine-contained polymers such as polytetrafluoroethylene (PTFE) and fluorinated ethylene-propylene (FEP)) is usually needed for a triboelectric airflow sensor, while their constraint conditions and contacts with electrodes may vary.

The flapping film can be connected with both the two electrodes, and only its central part vibrates in airflows. The periodic vibration of a flapping film is also accompanied by a continuous rubbing process against electrodes, leading to fluctuating negative charges on the flapping film and positive charges on electrodes. Based on this principle, Hu *et al.* developed an air-induced triboelectric nanogenerator (ATNG) to perceive airflows, equipped with a PTFE film and two pieces of conductive glasses to collect negative and positive charges, respectively (Fig. 6a and b).[48] To further improve the triboelectric performance, inductively coupled plasma (ICP) treatment was utilized to create nanostructures on the surfaces of PTFE films (Fig. 6b). Based on reasonable material designs and device structures, ATNG sensors could quantitatively respond to airflows with different flow rates (15–25 L min^{-1}) and relative humidities (20–100%), demonstrating their potential in sensing applications such as environmental monitoring and industrial manufacturing. In addition to the above device configuration with two ends of a flapping film connected with both electrodes, there are also device structures in which the flapping film is connected with neither of the electrodes. As

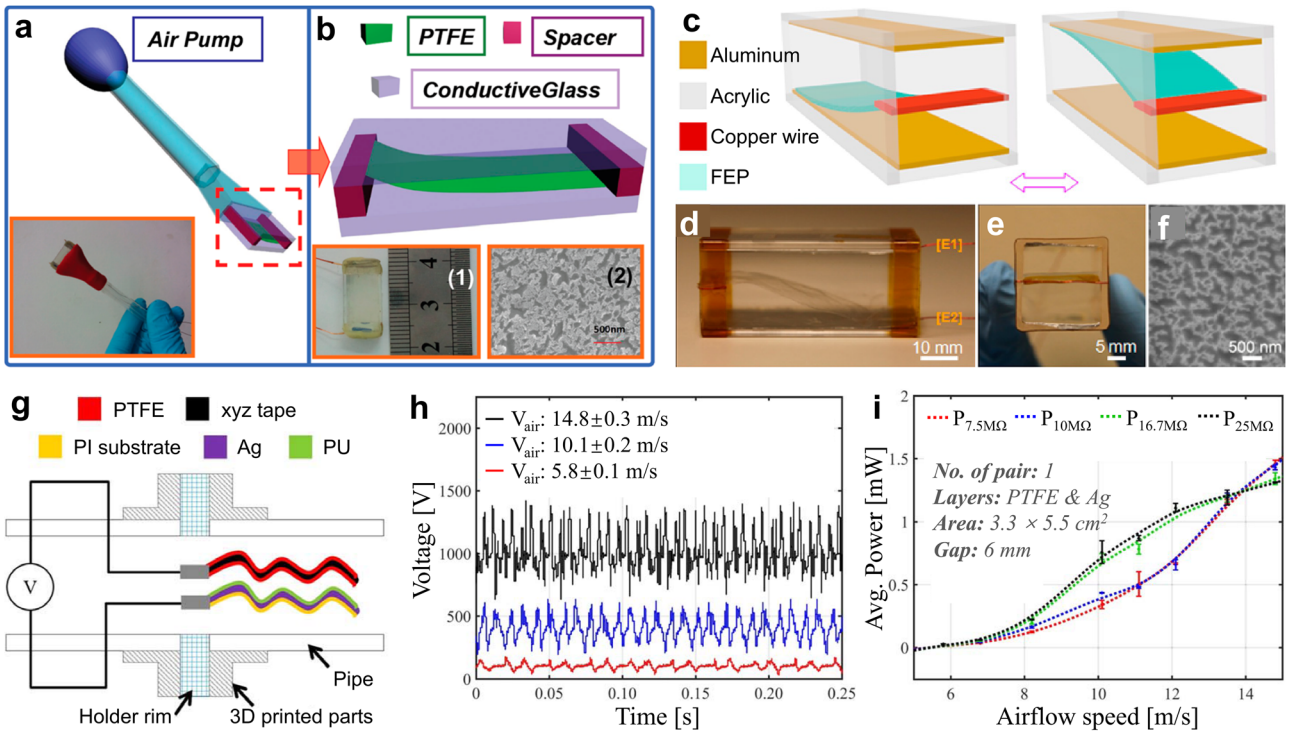

Fig. 6 Advanced triboelectric airflow sensors. (a) Schematic illustration of an ATNG sensor. (b) Enlarged schematic illustration, photograph and SEM image of an ATNG sensor. Reproduced with permission from ref. 48. Copyright 2014, American Chemical Society. (c) Schematic illustration of a TENG airflow sensor and its working mechanism. (d) and (e) Photographs and (f) SEM image of a TENG airflow sensor. Reproduced with permission from ref. 78. Copyright 2013, American Chemical Society. (g) Schematic illustration of the configuration of a flapping film generator. (h) Voltage responses of a flapping film generator under different airflow velocities. (i) Relationship between the power output and the gas velocity. Reproduced with permission from ref. 79. Copyright 2019, IOP Publishing.

shown in Fig. 6c, Wang *et al.* proposed a TENG airflow sensor composed of a FEP film and two aluminum foils, with the dimensions of 2.5 cm × 2.5 cm × 22 cm.[78] One end of the flexible FEP film was fixed at the middle of the wind channel, leaving the other end to vibrate freely in airflows. With the wind-induced resonance vibration, the flapping FEP film periodically rubs against aluminum electrodes and generates electrical signals, producing an output power up to 0.16 mW, and the triboelectric sensitivity was measured to be 0.09 μA m^{-1} s. Moreover, a self-powered wind vector sensor system consisting of four TENG airflow sensors arranged in four different directions was constructed to simultaneously monitor the wind speed and direction in real time, laying the foundation for advanced sensing systems and wind energy harvesting techniques. Aside from the above configurations, both the two electrodes can be designed to be flexible and flapping in airflows. Briand *et al.* reported a TENG airflow sensor consisting of two flapping films, which are polyurethane (PU)/silver/polyimide (PI) films and PTFE/XYZ tape films (Fig. 6g).[79] In this elaborately designed sensor, PU and PTFE served as positive and negative triboelectric materials, respectively, and silver/PI and XYZ tape functioned as supportive and conductive layers. In this way, the all-flexible TENG airflow sensor could sensitively respond to airflows, and the oscillation frequency and amplitude of the output voltage exhibited a positive correlation with gas velocity (Fig. 6h and i). The geometries of this TENG airflow sensor (film length, width, and spacing) was also optimized to achieve the maximum output power.

Triboelectric airflow sensors are noted for their features of simple structures, easy fabrication, and the great potential in energy harvesting, which have enabled many peripheral applications related to airflow sensing. However, the typical sizes of triboelectric airflow sensors are at the centimeter scale, which may bring great difficulties in their miniaturization. Besides, the working mechanism based on flapping films will cause a relatively lower accuracy, higher detection limit, and slower response speed (the response time cannot be shorter than the period of the flapping movement) and will inevitably bring periodic disturbance on flow fields.

3.1.5. Optical airflow sensors. With the emergence of micro- and nano-manufacturing, optical and optoelectronic devices with smaller sizes and delicate structures provide growing opportunities for the interdisciplinary research on airflow sensing, and expedite the development of sensors with novel working principles and higher performance. In general, optical airflow sensors can be divided into two categories according to their reading signals, which are optical signal-based sensors (with signals collected using spectrometers),[53,80–84] and electrical signal-based sensors (with signals collected using electrical meters).[27,82,85] Due to the diversity of optical airflow sensors, we will choose the typical examples for both of the two categories to briefly introduce

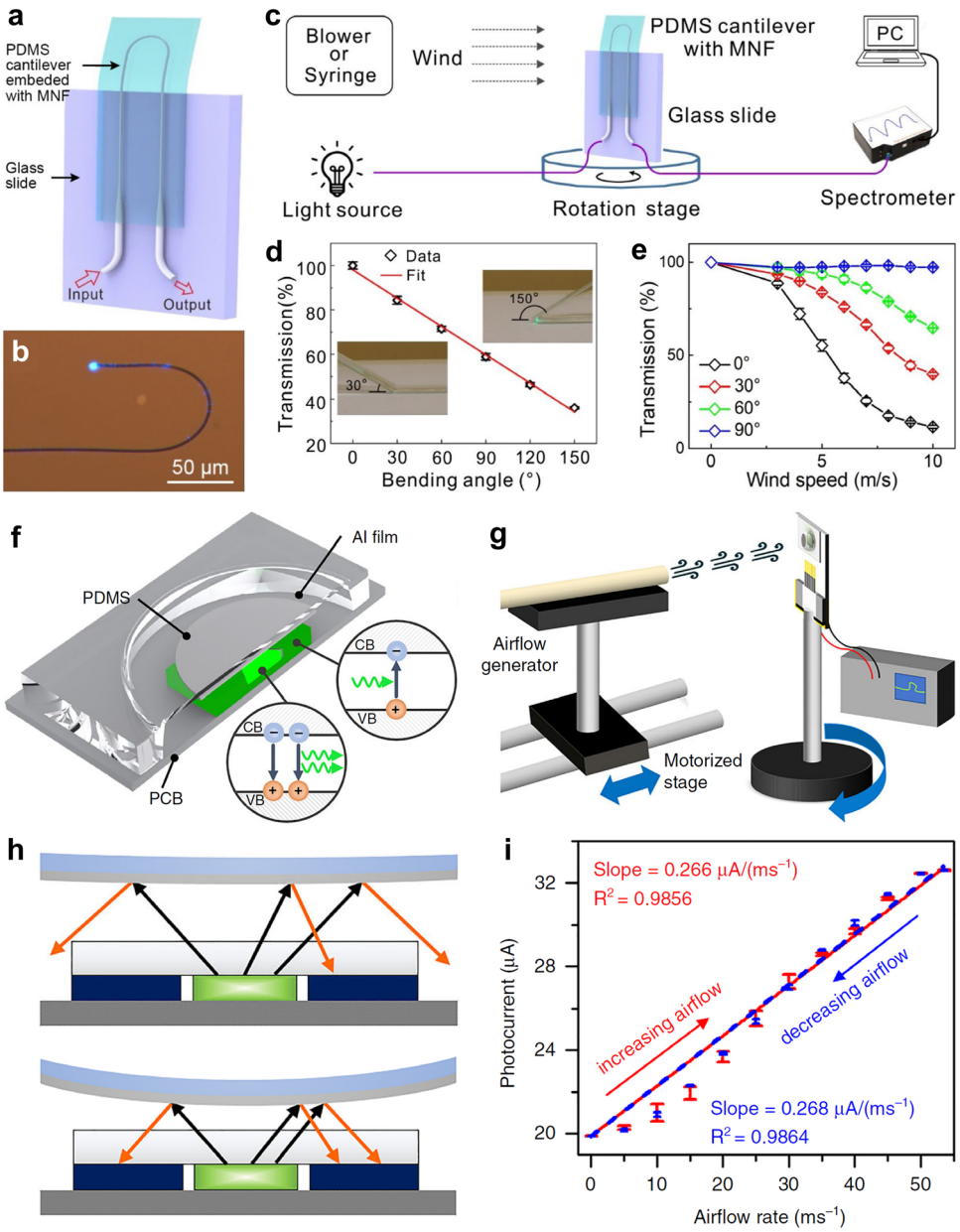

Fig. 7 Advanced optical airflow sensors. (a) Schematic illustration of a U-shaped MNF-enabled airflow sensor. (b) Optical microscopy photograph of an optical microfiber guiding a 473 nm laser. (c) Schematic illustration of the testing setup for measuring airflow responses. (d) Transmission as a function of bending angle. (e) Transmission as functions of wind speed and direction. Reproduced with permission from ref. 53. Copyright 2021, Springer Nature. (f) Schematic illustration of a chip-scale optical airflow sensor. (g) Schematic illustration of the experimental setup for measuring the responses to airflows. (h) Distributions of reflected light under airflows with low and high velocities. (i) Relationship between the photocurrent and the gas velocity. Reproduced with permission from ref. 27. Copyright 2022, Springer Nature.

their working mechanisms, design concepts, and sensing performances.

As for optical signal-based airflow sensors, Tong *et al.* utilized the transmission decrease of optical micro/nanofibers (MNF) when applied with deformations and proposed a novel airflow sensing element.[53] This sensing element was composed of a flexible polydimethylsiloxane (PDMS) cantilever embedded with a U-shaped MNF guiding a laser beam (Fig. 7a and b), which was used to monitor the real-time transmission of MNF at different gas velocities. As shown in Fig. 7c, when airflows were introduced, the free end of a PDMS cantilever along with the embedded MNF would accordingly bend, resulting in a decrease in the laser intensity delivered by the MNF, which was measured using a spectrometer. Since the relationship between the transmission and the bending angle was well-established (Fig. 7d), a clear relationship between the transmission and the wind speed, as well as the response curves under different wind directions, could be obtained (Fig. 7e). For electrical signal-based airflow sensors, Li *et al.* proposed chip-scale optical airflow sensors shown in Fig. 7f, integrated with GaN-based

LEDs (for both light emission and detection), droplet-shaped PDMS membranes (for generating deformations in airflows), and Al films (for reflecting the emitted light).[27] This device architecture enabled the direct reading of current signals because the built-in GaN-based LEDs served as photodetectors and converted light intensity into measurable photocurrents (Fig. 7g). Specifically, the GaN-based LED in the center served as the constant light source. The emitted light was reflected by the Al film attached on the inner surface of PDMS, and then detected by the surrounding GaN-based LEDs. When the gas velocity increased, PDMS and Al films deformed and became concave shapes, rendering that more photons irradiate the surrounding LEDs after the reflection, which would result in a larger photocurrent (Fig. 7h). In this way, the quantitative relationship between the photocurrent and the gas velocity was determined (Fig. 7i), showing a small hysteresis, a wide detection range (up to 53.5 m s^{-1}), and a short response time (12 ms).

Optical airflow sensors are generally featured with their unconventional working mechanisms and fast optical responses. Nevertheless, the coupled optical, electrical and mechanical elements bring more challenges to the reliability and stability of devices. Moreover, for optical signal-based airflow sensors, the use of spectrometers may cause cumbersome structures and bring difficulties in the device miniaturization.

The performances of the typical airflow sensors introduced in this review are listed in Table 1. Based on this table and our previous analysis, we briefly summarize the advantages and disadvantages of each type of airflow sensor. Thermal airflow sensors are featured with their short response times, wide detection ranges, and probably the greatest potential for miniaturization. Therefore, their structures have been significantly optimized with the assistance of several key techniques, making them promising in the highly integrated fields, such as unmanned aerial vehicles and electronic skins. Nevertheless, there are still challenges in the fabrication processes of thermal airflow sensors, which usually require expensive photolithography, sputtering and etching systems. Structural diversity can be a typical feature of piezoresistive sensors because of the multiple pathways for realizing the piezoresistive effect. With the great endeavor researchers have made in the structural design, piezoresistive airflow sensors exhibit a decent overall performance among various types of sensors. The incorporation of chemical treatments in some cases further lowered the cost and improved the universality. However, the sizes of most piezoresistive airflow sensors' functional parts are still very large (several square millimeters or even centimeters in area), which poses enormous challenges to their miniaturization and integration. Piezoelectric and triboelectric airflow sensors can produce voltage signals when applied with airflows without the introduction of power supplies, which is beneficial for realizing self-powered sensing systems. Their simple fabrication processes and low costs are also advantageous in many application scenarios. However, the processing and transducing of oscillating voltage signals is usually a prerequisite for these two types of airflow sensors, which may further complicate their device structures. Besides, for piezoelectric and triboelectric sensors based on the oscillation of their functional parts, a relatively higher gas speed is usually needed to start the oscillation, which inevitably increases the detection limits. As for optical airflow sensors, the ultrafast transformation processes from mechanical deformations to optical signals significantly shorten their response times, which may facilitate the

Table 1 Summary of the performances of typical airflow sensors

Name	Working mechanism	Sensitivity	Response time	Detection range	Ref.
Ni/W multi-layers deposited on NCD	Thermal	N/A	0.00068 s	0.5–30 m s^{-1}	32
Al or Pt wire	Thermal	0.196–1.61 V s m^{-1}	0.07 s	0.01–17.5 m s^{-1}	34
Pt films deposited on PI substrates	Thermal	N/A	0.1 s	0–6 m s^{-1}	11
Porous Ag nanosheets	Thermal	N/A	2 s	0.1–10 mL min^{-1}	86
Ti/Pt hot films	Thermal	N/A	N/A	0.1–6 m s^{-1}	31
ML-based flow sensors	Thermal	N/A	N/A	0–5.07 L min^{-1}	29
SiNW-BHS	Piezoresistive	9.9×10^{-5} m^{-2} s^2	0.040 s	0.15–13.77 m s^{-1}	38
SCNTNs	Piezoresistive	0.0124 s m^{-1}	0.021 s	0.11–5.51 m s^{-1}	87
SCNT-CNs	Piezoresistive	0.00652 s m^{-1}	0.021 s	0.02–21.22 m s^{-1}	28
CNTs/CSF	Piezoresistive	~0.005 s m^{-1}	1.3 s	0.05–3.5 m s^{-1}	41
GSEM	Piezoresistive	0.002–0.0912 s m^{-1}	1.04–1.28 s	0.0176–3.5 m s^{-1}	88
GCEF	Piezoresistive	(−0.043)–(+0.446) s m^{-1}	0.12–1.5 s	0.0087–23 m s^{-1}	60
CNTF-PPPS	Piezoresistive	N/A	0.2–0.35 s	0.1–4 m s^{-1}	65
SCFN	Piezoresistive	N/A	1.7 s	0.053–2.66 m s^{-1}	66
MMPF	Piezoelectric	N/A	0.57 s	0.5–10 m s^{-1}	45
SMPF	Piezoelectric	N/A	0.887 s	2.5–14 m s^{-1}	46
NMFs	Piezoelectric	83.3 mV m^{-1} s	N/A	3.2–19.8 m s^{-1}	47
PVDF cantilever array	Piezoelectric	N/A	0.02–0.025 s	0–14 m s^{-1}	67
PSF	Piezoelectric	15 mV m^{-1} s	0.03–0.2 s	0.3–16 m s^{-1}	68
PVDF cantilever	Piezoelectric	N/A	< 1 s	4.3–10.6 m s^{-1}	69
ATNG	Triboelectric	N/A	N/A	6.5–10.8 m s^{-1}	48
FEP films and Al foils	Triboelectric	0.09 mA m^{-1} s	N/A	~6–14 m s^{-1}	78
PU/Ag/PI and PTFE/XYZ tape	Triboelectric	N/A	N/A	5.8–14.8 m s^{-1}	79
MNF	Optical	−14.6% m^{-1} s	0.012 s	3–10 m s^{-1}	53
GaN chip with a PDMS membrane	Optical	0.268 μA m^{-1} s	0.012 s	0–53.5 m s^{-1}	27

application scenarios that require the capture of transient features, such as flow rate measurements and motion perception. To further realize the miniaturization and integration of optical airflow sensors, researchers should try to avoid using spectrometers with cumbersome volumes and employ other optical-to-electrical transformation approaches to measure the real-time gas speed.

3.2. Integrated sensing systems

Based on the development of high-performance airflow sensors functioning under different working principles, many researchers further endeavored to construct integrated systems with multiple sensors to boost their sensing performance and extend functionalities. In particular, several key concepts and techniques, such as MEMS,[17] IoT,[2] 3D printing,[89] and machine learning,[29] have enabled the precise fabrication of sensors with miniaturized structures, as well as the well-organized combination of their functions. Generally, advanced airflow sensors are integrated in two manners: (1) forming large-scale airflow sensor arrays to measure the spatially distributed gas speed and direction,[90–93] and (2) combining airflow sensors with other types of sensors to form a multifunctional sensing system.[11,94] The first pathway mainly focuses on the high-throughput collection of detailed information in flow fields, while the second one is more suitable for applications with higher complexity. In this section, we introduce the proceedings in both of the two aspects to give an overview of this interdisciplinary field.

The spatial detection of both the airflow speed and the direction is highly essential for many application scenarios. Therefore, the integration of multiple airflow sensors with ordered arrangements, uniform sensing performance and good signal readability becomes a prerequisite. To tackle the challenges in spatial airflow sensing, Dong *et al.* developed a spatial airflow impact source positioning system based on the MEMS fabrication of piezoresistive sensor arrays.[91] Boron-doped silicon MEMS sensors with well-defined structures were directly mounted on printed circuit boards, which were then fixed on flexible PDMS substrates in a 3 × 3 arrangement. By converting and processing the signals of this sensing system *via* a microcontroller unit (MCU) and a computer, the authors demonstrated the precise positioning of an impact source (*i.e.*, the gas jet) based on the physical models of wave propagation. Compared with 2 × 2 sensor arrays, the triaxial coordinate localization accuracies of 3 × 3 sensor arrays were improved by 96.9%, 87.8%, and 74.9%, respectively. The flexible PDMS substrates also enabled good wearability, which were expected to provide solutions for the development of high-performance wearable electronics. This basic concept of constructing airflow sensor arrays has been widely reported for the purpose of collecting spatially distributed velocities in the flow fields,[31,38,90,92,93] while the perception of some other properties (*e.g.*, pressure) may further provide rich information carried by airflows.

Faced with the growing need in the airflow perception for small unmanned aerial vehicles (SUAVs), Jiang *et al.* proposed ultrathin all-PI flexible skins integrated with piezoresistive airflow sensors and capacitive pressure sensors.[94] The as-proposed flexible skins were generally composed of PI trilayers with rationally designed structures, including piezoresistors, cantilevers, micro-channels, cavities, and electrodes. A velocity resolution of 2.4 m s^{-1} and a pressure resolution of 4.5 Pa were achieved by this all-PI trilayer structure, laying the foundation for the precise sensing and device integration. Moreover, the integrated skins could be attached to curved surfaces such as airfoil models, so as to perceive the near-surface flow fields. With the assistance of a multilayer perceptron neural network model, the pressure and airflow data were directly correlated with flight parameters (*e.g.*, airspeed, angle of attack (AOA), and angle of sideslip (AOS)), exhibiting low errors for AOA (0.67°) and airspeed (0.73 m s^{-1}). Endowed with flexible structures, decent sensing performance and reliable signal processing methods, such integrated sensing systems are expected to be used for analyzing the flight dynamics of SUAVs. Chen *et al.* also developed a bionic adaptive thin-membrane sensory system consisting of multiple graphene/single-walled nanotube-Ecoflex membrane (GSEM) based airflow sensors.[88] High-performance GSEM-based airflow sensors could be attached to arbitrary curved surfaces and produce nearly identical airflow responses, providing a solid foundation for their large-scale integration. In this way, GSEM-based airflow sensors were applied to a smart window system to realize the intelligent, open, and close behaviors *via* a threshold control. In addition, 4 × 4 and 2 × 2 GSEM-based airflow sensor arrays were utilized to precisely perceive the spatial distribution of gas velocity (Fig. 8a–c), and manipulate a wireless vehicle in a noncontact mode, respectively. In another work, they demonstrated an artificial intelligent spiderweb (AISW) array system with eight individual airflow sensors to show its capability in precisely acquiring the intensity, direction, and location information of airflows, which were expected to realize active warning and non-contact control.[60]

Furthermore, if sensors with more functions are integrated into a system, more complicated working scenarios can be enabled, such as artificial electronic skins (e-skins). For instance, Zhu *et al.* designed a flexible and multifunctional e-skin based on patterned thermal sensor arrays fabricated on a PI substrate (Fig. 8d).[11] As shown in Fig. 8e, two types of sensor configurations were employed, *i.e.*, exposed sensors (for temperature and airflow sensing) and covered sensors (for matter and pressure sensing). The peripheral Pt wires with a larger resistance (550 Ω) were defined as cold films, which served as thermoresistors to perceive the ambient temperature. The Pt wires in the center, designed with a much lower resistance (124 Ω), were defined as hot films and served as airflow, matter, and pressure sensors through the Joule heating. Aside from the above-mentioned working mechanisms of hot-film airflow sensors, it should be noted that the sensing of matters and pressure utilized the variations in the fluxes of conductive heat transfer upon applying matters or pressure on hot films, which are highly similar to the thermosensation behaviors of human skins. By combining these sensing units, this e-skin achieved the simultaneous and accurate acquisition of multiple

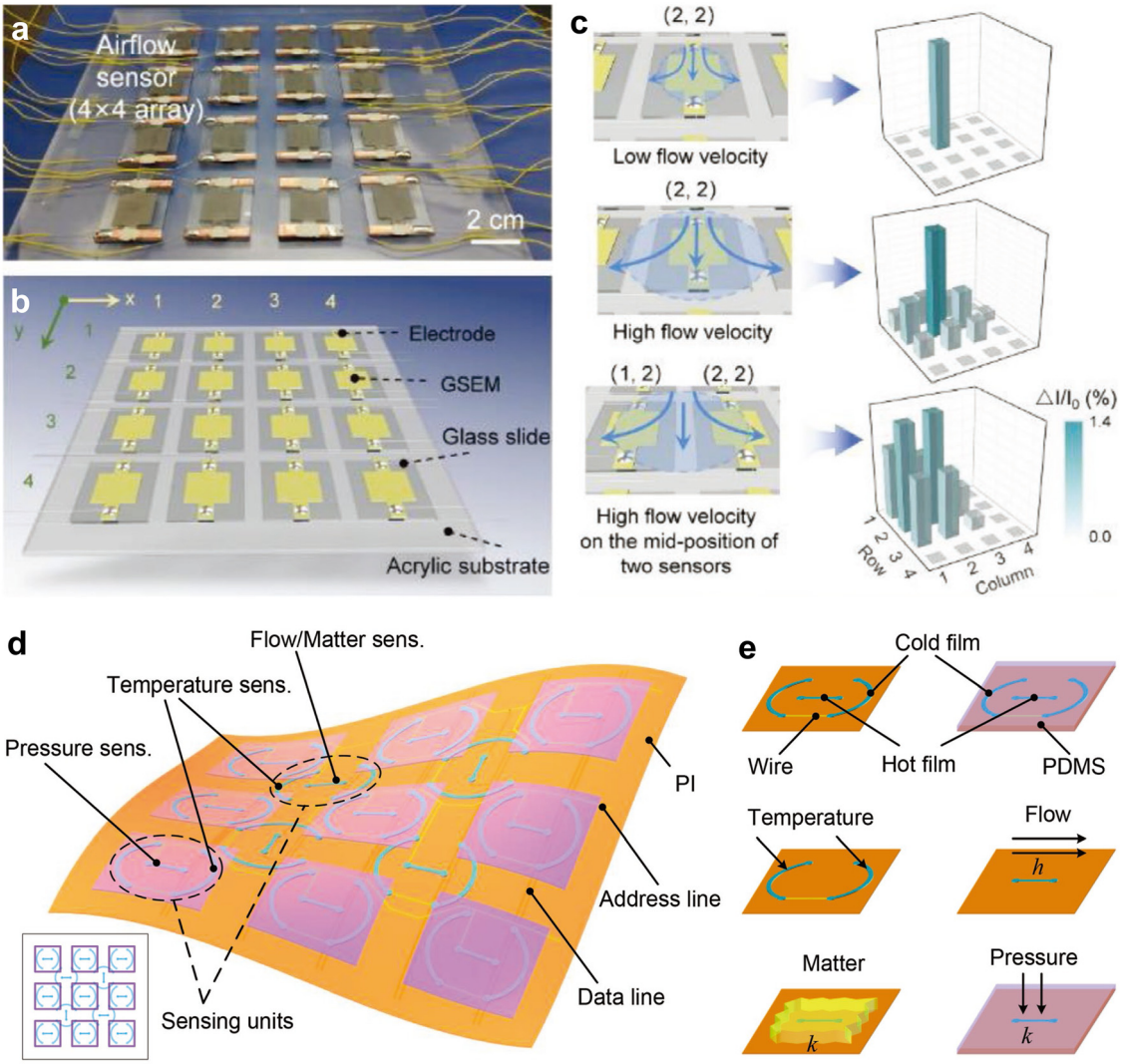

Fig. 8 Integrated sensing systems of airflow sensors. (a) Photograph and (b) schematic illustration of a 4 × 4 GSEM-based airflow sensor array. (c) Spatial distribution of the airflow derived from the 4 × 4 GSEM-based airflow sensor array. Reproduced with permission from ref. 88. Copyright 2021, Wiley-VCH. (d) Schematic illustration of a flexible and multifunctional e-skin. (e) Designs of the sensing units, including temperature, flow, matter, and pressure sensors. Reproduced with permission from ref. 11. Copyright 2017, Wiley-VCH.

sensing signals without significantly increasing the device complexity.

In brief, a higher level of miniaturization, integration and multi-functionalization of advanced airflow sensors and other sensors is anticipated to be realized with the ramping development of novel techniques, while challenges still remain in the aspects of sensor performance, system robustness, signal processing efficiency, *etc.* With the gradual maturing of this field, researchers are paying more and more attention to the reliability of functions from a systematic perspective, rather than focusing on the specific performance of individual sensors.

3.3. Application demonstrations

With the rational design and controlled fabrication of airflow sensors with desired sensing performance and extended functionalities, researchers have made application demonstrations in various scenarios, such as respiratory monitoring,[20,27,28,39,40,53,65,90,95,96] flow rate measurement,[28,77] and motion and environment perception,[17,31,41,58,66,92,94,97] to elucidate the possible practical prospects. Based on these advances, other branch applications have also been derived, including precision instruments,[98,99] acoustic sensing and voice recognition,[39,53,95,96] airplane flight control,[100,101] weather observation,[102,103] *etc.* Although there still exist some issues (mass production, encapsulation, signal transduction, *etc.*) for realizing their real-life applications, it is still worth noting the exciting advances made in this area, which may evoke more needs and bring more insights into the development of healthcare, human–computer interaction, industrial production, *etc.*[8–10,12–14]

Respiratory behavior is an important aspect in health monitoring, relying on the real-time and precise measurement of inhalation and exhalation,[25] which can be facilely achieved using advanced airflow sensors. For instance, our group

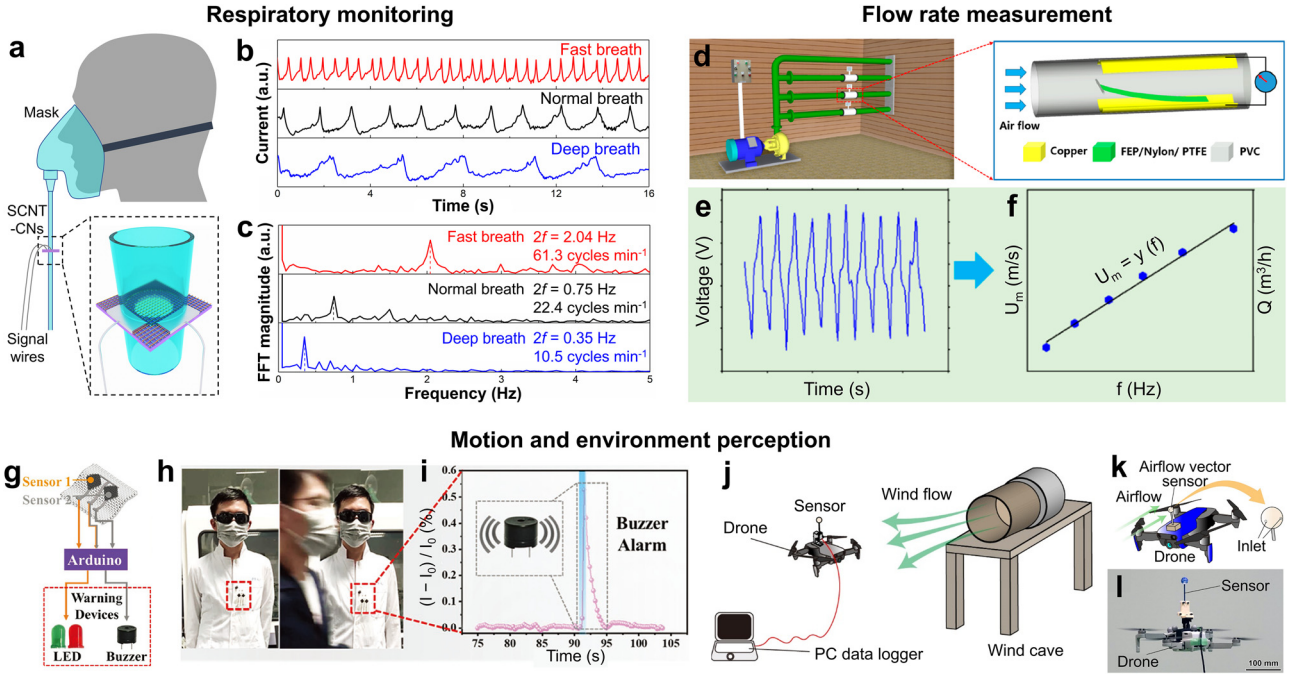

Fig. 9 Application demonstrations of airflow sensors. (a) Schematic illustration of a respiratory monitor consisting of a SCNT-CN-based airflow sensor. (b) Time-domain and (c) frequency-domain signals obtained using a respiratory monitor. Reproduced with permission from ref. 28. Copyright 2024, American Chemical Society. (d) Schematic illustration of the flow rate measurement realized using a triboelectric airflow sensor. (e) Voltage output and (f) response characteristics (dependence of gas velocity and flow rate on the voltage frequency) of a triboelectric airflow sensor. Reproduced with permission from ref. 77. Copyright 2020, MDPI. (g) Integrated airflow detection system composed of CNT/CSF airflow sensors, Arduino modules, and warning devices. (h) Photographs of a person passing by a blind person equipped with an integrated airflow detection system. (i) Electrical responses and the buzzer alarm obtained from this system. Reproduced with permission from ref. 41. Copyright 2020, Wiley-VCH. (j) Experimental setup for measuring the airflow responses of a sensor mounted on a drone. (k) Schematic illustration and (l) photograph of a drone mounted with an airflow sensor for perceiving the environment and measuring movements. Reproduced with permission from ref. 92. Copyright 2022, MDPI.

encapsulated an SCNT-CN-based airflow sensor in a pipe connected with a face mask to construct a simple respiratory monitoring system (Fig. 9a).[28] With the electrical signals amplified using a field-effect transistor, this respiratory monitoring system could respond quickly to the respiratory behavior of the volunteer and output real-time signals for fast, normal and deep breaths (Fig. 9b). The subsequent FFT processing of the time-domain signals could also enable the acquisition of breath frequencies, which further enriched the respiratory information (Fig. 9c). Some other works directly set airflow sensors in front of the person's nose or mouth for perceiving breaths, rather than encapsulating them into pipes.[39,65] For example, Tong *et al.* directly mounted their MNF-enabled airflow sensor in a facial mask to measure the respiratory responses, obtaining clear characteristics for breaths with different frequencies and inhalation/exhalation volumes.[53] This configuration has the obvious advantage of easy implementation, whereas it is more demanding on the robustness of airflow sensors against external forces.

As the devices measuring gas velocities, well-calibrated airflow sensors also have the potential to replace some of the conventional flow meters used in industries and heating, ventilation, and air conditioning (HVAC).[104] Ma *et al.* demonstrated the incorporation of a triboelectric airflow sensor into pipelines to measure the flow rates (Fig. 9d).[77] The ultrathin structures of electrodes significantly reduced the flow resistance, and the high flexibility of flapping films facilitated the sensitive responses to gas flows. By reading the periodic voltage signals generated using a triboelectric airflow sensor, the corresponding oscillation frequency could be quantitatively correlated with the gas velocity and flow rate, which lays the foundation for practical flow rate measurements (Fig. 9e and f). Similarly, our SCNT-CN-based airflow sensors could also enable the monitoring of the flow rate when encapsulated in pipelines.[28] With the assistance of Arduino modules, the flow rate measuring system could accurately display the real-time flow rate and exhibit rapid responses to the sudden changes in the flow rate, which would be of vital importance for analyzing and adjusting the parameters of a proportional-integral-derivative (PID) control process.

Motion and environment perception is essential for various scenarios involving moving objects, such as the security of disabled people, the attitude and motion control of unmanned aerial vehicles, *etc.*[50] A swift response to the speed and direction variations of airflows is beneficial for timely acquiring the changes in the environment or in the object's own motion. Then, the integrated alarm system or the driving system will react based on the airflow responses. As a demonstration, Zhang *et al.* constructed an integrated airflow detection system consisting of CNT/CSF airflow sensors, Arduino modules, and

warning devices (Fig. 9g), which could be fabricated on wearable fabrics.[41] When a moving object passed a person wearing this detection system (Fig. 9h), the sensing part would produce strong and sharp signals that could trigger the functioning of warning devices (Fig. 9i). This demonstration shows the potential of this integrated airflow detection system in ensuring blind people's safety. In addition to the application in wearable devices, airflow sensors can also be combined with unmanned aerial vehicles to perceive motions and improve flight stability. Takahashi *et al.* mounted a compact spherical airflow sensor on a drone to realize the sensing of the 2D wind direction and speed (Fig. 9j–l).[92] The sensor output agreed well with the real airflows in the environment, verifying its outstanding robustness and accuracy in practical applications.

4. Summary and outlook

In this review, we summarized the general working mechanisms, functional materials, and device configurations of advanced airflow sensors and their integrated sensing systems and application demonstrations. Although exciting proceedings are listed, significant challenges still exist in the aspects of structural design, material synthesis, function integration, and practical applications. More theoretical, experimental, or even industrial breakthroughs are awaiting to be accomplished for the further development of airflow sensors. Herein, in the final section, we attempt to identify the major challenges and propose several directions for this area.

The primary challenge lies in the identification of promising functional materials. On the one hand, with the fast development of condensed matter physics, materials science, and synthetic chemistry, the library of potential functional materials for airflow sensing has been largely extended in recent decades. On the other hand, faced with multiple working mechanisms, researchers need to select the most suitable working mechanism for their application scenarios and rationally screen the functional materials to optimize the sensing performance. Considering the great complexity in materials' selection, several novel strategies and methodologies, such as first-principles calculations, big data, and ML, should be comprehensively employed. With the assistance of these theoretical approaches, tedious screening experiments may be significantly reduced, and the performance of the selected materials may also be fully optimized.

Serious challenges are also met in the controlled synthesis of functional materials and the high precision fabrication of devices. Abundant examples have shown the intricate impacts of multi-scale structures on the resultant sensing performance, indicating the essential role of controlled synthesis and fabrication. Researchers may consider both bottom-up and top-down approaches to obtain desired structures in future studies. The bottom-up pathway requires an atomic- or nano-level control over the structures of functional materials, which can be realized by comprehensively optimizing the synthetic conditions in chemical/physical vapor deposition, atomic layer deposition, and other wet chemistry methods. As a supplement, top-down methods, such as 3D printing and MEMS processing, are expected to effectively control the meso- and macro-structures of airflow sensors.

From the view of device designs, reasonable device configurations guided by concrete theories are also urgently needed. An ideal device configuration should not only maximize the sensing performance of functional materials, but also improve the flexibility, robustness, practicality, and compatibility with other sensing modules in an integrated system. Faced with these challenges, biomimetic designs (*e.g.*, spiderweb and fluffy hair) have been extensively proposed to verify their outstanding performance.[41,60] However, aside from phenomenologically learning from nature, more quantitative theories and calculations should also be explored to meet the growing needs in the aspects of airflow sensing performance, multifunctionality, and system integration. For instance, computational tools capable of solving multi-physical fields (mechanics, fluid dynamics, electromagnetics, *etc.*) should be utilized in the design processes. Based on accurate calculations, the structures of individual airflow sensors and the arrangement of multiple sensors are expected to be largely optimized.

For the integrated sensor systems, there are growing demands in the real-time signal collection, data analysis, output display, and human–computer interaction, especially in the fields of healthcare and wearable electronics. To simultaneously achieve these goals, researchers should leverage the advantages of interdisciplinary study to develop advanced systems with more functions, miniaturized sizes, lower power consumptions, lower costs, anti-interference ability, biocompatibility, *etc.*

Finally, the commercialization of airflow sensors strongly depends on mature fabrication processes, standardized testing protocols, uniform sensing performances, well-controlled costs, *etc.*, which can be great challenges to the novel airflow sensors reported in research papers. To promote the widespread application in the commercial market, industrial standards should be more considered and embodied in the design and fabrication of airflow sensors. Researchers are expected to use functional materials that can be synthesized and processed in large quantities to control the costs, and make the resultant sensors more compatible with the standardized power input/out and data readout. For biological related applications (*e.g.*, healthcare), the issue of biocompatibility should also be carefully considered.

Author contributions

R. Zhang directed the whole project. Q. Jiang wrote the paper. K. Leu, F. Wang, R. Li, K. Wang, Y. Zhao, A. Xi, and Y. Zang revised the paper.

Data availability

No primary research results, software or code have been included and no new data were generated or analysed as part of this review.

Conflicts of interest

There are no competing interests to declare.

Acknowledgements

This work is supported by the National Key Research and Development Program (Grant No. 2020YFC2201103 and 2020YFA0210702) and the National Natural Science Foundation of China (Grant No. 22075163).

References

1 M. A. Jamshed, K. Ali, Q. H. Abbasi, M. A. Imran and M. Ur-Rehman, *IEEE Sens. J.*, 2022, **22**, 5482–5494.
2 J.-L. Bayo-Monton, A. Martinez-Millana, W. Han, C. Fernandez-Llatas, Y. Sun and V. Traver, *Sensors*, 2018, **18**, 1851.
3 M. S. Al-kahtani, F. Khan and W. Taekeun, *Sensors*, 2022, **22**, 5738.
4 A. Tsanousa, E. Bektsis, C. Kyriakopoulos, A. G. González, U. Leturiondo, I. Gialampoukidis, A. Karakostas, S. Vrochidis and I. Kompatsiaris, *Sensors*, 2022, **22**, 1734.
5 A. Kumar, *Manuf. Lett.*, 2018, **15**, 122–125.
6 Y.-H. Wang, C.-P. Chen, C.-M. Chang, C.-P. Lin, C.-H. Lin, L.-M. Fu and C.-Y. Lee, *Microfluid. Nanofluid.*, 2009, **6**, 333–346.
7 J. Tao and X. Yu, *Smart Mater. Struct.*, 2012, **21**, 113001.
8 B. Cheng and P. Wu, *ACS Nano*, 2021, **15**, 8676–8685.
9 L. Ribeiro, O. Saotome, R. d'Amore and R. de Oliveira Hansen, *Sensors*, 2022, **22**, 3484.
10 D. Zhang, W. Yang, W. Gong, W. Ma, C. Hou, Y. Li, Q. Zhang and H. Wang, *Adv. Mater.*, 2021, **33**, 2100782.
11 S. Zhao and R. Zhu, *Adv. Mater.*, 2017, **29**, 1606151.
12 F. Liu, Y. Zhao, N. Xie, Y. Wang, M. Liu, Z. Han and T. Hou, *Nanoscale*, 2024, **16**, 4299–4307.
13 M. H. Chung, S. Yoo, W.-N. Jung, H. Jeong and K.-H. Yoo, *Adv. Fiber Mater.*, 2023, **5**, 1788–1798.
14 Y. Cheng, B. Jiang, S. Chaemchuen, F. Verpoort and Z. Kou, *Carbon Neutralization*, 2023, **2**, 213–234.
15 R. G. Folsom, *Trans. ASME*, 2022, **78**, 1447–1460.
16 J. X. Zhang, *AIP Adv.*, 2017, **7**, 065315.
17 W. Xu, X. Wang, Z. Ke and Y. K. Lee, *IEEE Trans. Ind. Electron.*, 2022, **69**, 3183–3192.
18 Y.-F. Liu, P. Huang, Y.-Q. Li, Q. Liu, J.-K. Tao, D.-J. Xiong, N. Hu, C. Yan, H. Wang and S.-Y. Fu, *J. Mater. Chem. A*, 2019, **7**, 1889–1896.
19 Z. Wang, Y. Wang, Q. Gao, G. Bao, T. Cheng and Z. L. Wang, *Adv. Mater. Technol.*, 2023, **8**, 2201029.
20 J. Park, Y. Lee, J. Hong, M. Ha, Y.-D. Jung, H. Lim, S. Y. Kim and H. Ko, *ACS Nano*, 2014, **8**, 4689–4697.
21 H. Wang, H. Wang, S. Zhang, Y. Zhang, K. Xia, Z. Yin, M. Zhang, X. Liang, H. Lu, S. Li, J. Zhang and Y. Zhang, *Nano Res.*, 2022, **15**, 2576–2581.
22 W. Xu, L. Hong, X. Pan and Izhar, *IEEE Trans. Instrum. Meas.*, 2024, **73**, 1–9.
23 F. Ejeian, S. Azadi, A. Razmjou, Y. Orooji, A. Kottapalli, M. Ebrahimi Warkiani and M. Asadnia, *Sens. Actuators, A*, 2019, **295**, 483–502.
24 J. T. W. Kuo, L. Yu and E. Meng, *Micromachines*, 2012, **3**, 550–573.
25 I. Costanzo, D. Sen, L. Rhein and U. Guler, *IEEE Rev. Biomed. Eng.*, 2022, **15**, 103–121.
26 Q. Jiang, R. Li, F. Wang, X. Shi, F. Chen, Y. Huang, B. Wang, W. Zhang, X. Wu, F. Wei and R. Zhang, *Adv. Mater.*, 2022, **34**, 2107062.
27 Y. Luo, X. An, L. Chen and K. H. Li, *Microsyst. Nanoeng.*, 2022, **8**, 4.
28 Q. Jiang, K. Leu, X. Gong, F. Wang, R. Li, K. Wang, P. Zhu, Y. Zhao, Y. Zang and R. Zhang, *ACS Appl. Mater. Interfaces*, 2024, **16**, 20949–20958.
29 S. Shin, K. Baek, Y. Choi and H. So, *Adv. Intell. Syst.*, 2024, **6**, 2300711.
30 A. Al-Salaymeh and M. D. S. Ashhab, *Sens. Actuators, A*, 2006, **126**, 7–14.
31 H. Liu, N. Lin, S. Pan, J. Miao and L. K. Norford, *IEEE Sens. J.*, 2013, **13**, 1914–1920.
32 A. Talbi, L. Gimeno, J. C. Gerbedoen, R. Viard, A. Soltani, V. Mortet, V. Preobrazhensky, A. Merlen and P. Pernod, *J. Micromech. Microeng.*, 2015, **25**, 125029.
33 T. Dinh, H.-P. Phan, T.-K. Nguyen, A. Qamar, A. R. M. Foisal, T. Nguyen Viet, C.-D. Tran, Y. Zhu, N.-T. Nguyen and D. V. Dao, *J. Mater. Chem. C*, 2016, **4**, 10061–10068.
34 M. M. Sadeghi, R. L. Peterson and K. Najafi, *J. Micromech. Microeng.*, 2013, **23**, 085017.
35 T. Dinh, H.-P. Phan, T.-K. Nguyen, A. Qamar, P. Woodfield, Y. Zhu, N.-T. Nguyen and D. V. Dao, *J. Phys. D: Appl. Phys.*, 2017, **50**, 215401.
36 S. Zhang, L. Lou and C. Lee, *Appl. Phys. Lett.*, 2012, **100**, 023111.
37 S. S. Kumar and B. D. Pant, *Microsyst. Technol.*, 2014, **20**, 1213–1247.
38 S. Huang, B. Zhang, Y. Lin, C.-S. Lee and X. Zhang, *Nano Lett.*, 2021, **21**, 4684–4691.
39 P. Nie, R. Wang, X. Xu, Y. Cheng, X. Wang, L. Shi and J. Sun, *ACS Appl. Mater. Interfaces*, 2017, **9**, 14911–14919.
40 Y. Song, L. Chen, Q. Yang, G. Liu, Q. Yu, X. Xie, C. Chen, J. Liu, G. Chao, X. Chen and M.-W. Chang, *ACS Appl. Nano Mater.*, 2023, **6**, 8937–8944.
41 H. Wang, S. Li, Y. Wang, H. Wang, X. Shen, M. Zhang, H. Lu, M. He and Y. Zhang, *Adv. Mater.*, 2020, **32**, 1908214.
42 G.-H. Feng and P.-C. Su, *J. Micromech. Microeng.*, 2022, **32**, 015009.
43 M. C. Sekhar, E. Veena, N. S. Kumar, K. C. B. Naidu, A. Mallikarjuna and D. B. Basha, *Cryst. Res. Technol.*, 2023, **58**, 2200130.
44 Q. Liu, X.-X. Wang, W.-Z. Song, H.-J. Qiu, J. Zhang, Z. Fan, M. Yu and Y.-Z. Long, *ACS Appl. Mater. Interfaces*, 2020, **12**, 8288–8295.
45 Y. Bian, Y. Zhang and X. Xia, *J. Bionic Eng.*, 2016, **13**, 416–425.

46 Y. Bian, R. Liu and S. Hui, *Funct. Mater. Lett.*, 2016, **09**, 1650001.
47 Y.-K. Fuh, P.-C. Chen, Z.-M. Huang and H.-C. Ho, *Nano Energy*, 2015, **11**, 671–677.
48 H. Guo, J. Chen, L. Tian, Q. Leng, Y. Xi and C. Hu, *ACS Appl. Mater. Interfaces*, 2014, **6**, 17184–17189.
49 D. Kim, J. Lee, M. K. Park and S. H. Ko, *Commun. Mater.*, 2024, **5**, 41.
50 X. Pu, S. An, Q. Tang, H. Guo and C. Hu, *iScience*, 2021, **24**, 102027.
51 M.-J. Yin, B. Gu, Q.-F. An, C. Yang, Y. L. Guan and K.-T. Yong, *Coord. Chem. Rev.*, 2018, **376**, 348–392.
52 M. Ramakrishnan, G. Rajan, Y. Semenova and G. Farrell, *Sensors*, 2016, **16**, 99.
53 Z. Zhang, Y. Kang, N. Yao, J. Pan, W. Yu, Y. Tang, Y. Xu, L. Wang, L. Zhang and L. Tong, *Adv. Fiber Mater.*, 2021, **3**, 359–367.
54 V. Balakrishnan, H.-P. Phan, T. Dinh, D. V. Dao and N.-T. Nguyen, *Sensors*, 2017, **17**, 2061.
55 C.-H. Wu, D. Kang, P.-H. Chen and Y.-C. Tai, *Sens. Actuators, A*, 2016, **241**, 135–144.
56 M. R. Maschmann, B. Dickinson, G. J. Ehlert and J. W. Baur, *Smart Mater. Struct.*, 2012, **21**, 094024.
57 J. Choi and J. Kim, *Nanotechnology*, 2010, **21**, 105502.
58 L. Huang, Y. Liu, G. Li, Y. Song, J. Su, L. Cheng, W. Guo, G. Zhao, H. Shen, Z. Yan, B. Z. Tang and R. Ye, *Nano Lett.*, 2023, **23**, 597–605.
59 J. Chen, V.-T. Tran, H. Du, J. Wang and C. Chen, *Micromachines*, 2021, **12**, 504.
60 W. Zhou, P. Xiao, C. Zhang, Q. Yang and T. Chen, *Mater. Horiz.*, 2023, **10**, 1264–1273.
61 A. R. Aiyar, C. Song, S.-H. Kim and M. G. Allen, *Smart Mater. Struct.*, 2009, **18**, 115002.
62 Q. Jiang, F. Wang, R. Li, B. Li, N. Wei, N. Gao, H. Xu, S. Zhao, Y. Huang, B. Wang, W. Zhang, X. Wu, S. Zhang, Y. Zhao, E. Shi and R. Zhang, *Nano Lett.*, 2023, **23**, 523–532.
63 Q. Jiang, Y. Wu, F. Wang, P. Zhu, R. Li, Y. Zhao, Y. Huang, X. Wu, S. Zhao, Y. Li, B. Wang, D. Gao and R. Zhang, *Adv. Mater.*, 2024, **36**, 2402257.
64 R. Li, Q. Jiang, F. Wang, X. Shi, F. Chen, Y. Huang, B. Wang, W. Zhang, X. Wu, F. Wei and R. Zhang, *Small Methods*, 2022, **6**, 2101333.
65 T. Qi, C. Chen, Z. Yong, X. Gong and S. Ramakrishna, *Adv. Mater. Interfaces*, 2023, **11**, 2300077.
66 C. Shen, S. Sun, H. Zhang and Z. Zhang, *Adv. Mater. Technol.*, 2023, **8**, 2200571.
67 J. Hu, H. Peng and X. Yao, *Rev. Sci. Instrum.*, 2018, **89**, 085007.
68 J. Hu, J. Chen, P. Liu, S. Fan and W. Duan, *Sens. Actuators, A*, 2022, **336**, 113399.
69 J. Hu, H. Peng, T. Mao, T. Liu, M. Guo, P. Lu, Y. Bai and C. Zhao, *Flow Meas. Instrum.*, 2019, **67**, 166–175.
70 F.-R. Fan, Z.-Q. Tian and Z. Lin Wang, *Nano Energy*, 2012, **1**, 328–334.
71 X. P. Fu, T. Z. Bu, F. B. Xi, T. H. Cheng, C. Zhang and Z. L. Wang, *ACS Appl. Mater. Interfaces*, 2017, **9**, 32352–32358.
72 Z. Wang, Y. Yu, Y. Wang, X. Lu, T. Cheng, G. Bao and Z. L. Wang, *ACS Nano*, 2020, **14**, 5981–5987.
73 M. Xu, Y.-C. Wang, S. L. Zhang, W. Ding, J. Cheng, X. He, P. Zhang, Z. Wang, X. Pan and Z. L. Wang, *Extreme Mech. Lett.*, 2017, **15**, 122–129.
74 Y. Su, G. Xie, T. Xie, H. Zhang, Z. Ye, Q. Jing, H. Tai, X. Du and Y. Jiang, *J. Phys. D: Appl. Phys.*, 2016, **49**, 215601.
75 Y. Wang, E. Yang, T. Chen, J. Wang, Z. Hu, J. Mi, X. Pan and M. Xu, *Nano Energy*, 2020, **78**, 105279.
76 J. Hu, X. Pu, H. Yang, Q. Zeng, Q. Tang, D. Zhang, C. Hu and Y. Xi, *Nano Res.*, 2019, **12**, 3018–3023.
77 T. K. Phan, S. Wang, Y. Wang, H. Wang, X. Xiao, X. Pan, M. Xu and J. Mi, *Sensors*, 2020, **20**, 729.
78 Y. Yang, G. Zhu, H. Zhang, J. Chen, X. Zhong, Z.-H. Lin, Y. Su, P. Bai, X. Wen and Z. L. Wang, *ACS Nano*, 2013, **7**, 9461–9468.
79 R. I. Haque and D. Briand, *Smart Mater. Struct.*, 2019, **28**, 085002.
80 M. S. Cheri, H. Latifi, F. B. A. Aghbolagh, O. R. R. Naeini, M. Taghavi and M. Ghaderi, *Appl. Opt.*, 2013, **52**, 3420–3427.
81 C. L. Lee, C. X. Yang, T. Y. Liang and C. T. Ma, *IEEE Photonics Technol. Lett.*, 2019, **31**, 1775–1778.
82 F. Xing, G.-X. Meng, Q. Zhang, L.-T. Pan, P. Wang, Z.-B. Liu, W.-S. Jiang, Y. Chen and J.-G. Tian, *Nano Lett.*, 2014, **14**, 3563–3569.
83 P. Wang, Y. Zhao, Y. Yang and D.-J. Bi, *Sens. Actuators, A*, 2015, **221**, 29–32.
84 X. Wang, X. Dong, Y. Zhou, Y. Li, J. Cheng and Z. Chen, *Sens. Actuators, A*, 2014, **214**, 230–233.
85 F. Xing, Y. Yang, J. Shen, W. Jiang, Z. Liu, S. Zhu and X. Yuan, *Sens. Actuators, B*, 2016, **235**, 474–480.
86 E. Marzbanrad, B. Zhao and N. Y. Zhou, *Nanotechnology*, 2015, **26**, 445501.
87 Q. Jiang, F. Wang, R. Li, X. Wu, W. Zhang, S. Zhao, Y. Huang, B. Wang, S. Zhang, Y. Zhao and R. Zhang, *Adv. Funct. Mater.*, 2023, **33**, 2212665.
88 W. Zhou, P. Xiao, Y. Liang, Q. Wang, D. Liu, Q. Yang, J. Chen, Y. Nie, S.-W. Kuo and T. Chen, *Adv. Funct. Mater.*, 2021, **31**, 2105323.
89 T. Koutsis, P. Pikasis, A. Psyrris and G. Kaltsas, *Microelectron. Eng.*, 2020, **226**, 111286.
90 T. Jiang, L. Deng, W. Qiu, J. Liang, Y. Wu, Z. Shao, D. Wang, M. Zhang, X. Qian, J. Zhong, X. Wang and L. Lin, *Biosens. Bioelectron.*, 2020, **163**, 112288.
91 J. Wu, J. Cheng, C. Liu, M. Wang, D. Hao, Y. Mu, H. Wang, L. Cheng, B. Weng, W. Yang and L. Dong, *IEEE Sens. J.*, 2023, **23**, 19995–20001.
92 K. Haneda, K. Matsudaira, R. Noda, T. Nakata, S. Suzuki, H. Liu and H. Takahashi, *Sensors*, 2022, **22**, 1087.
93 N. André, B. Rue, G. Scheen, D. Flandre, L. A. Francis and J.-P. Raskin, *Sens. Actuators, A*, 2014, **206**, 67–74.
94 Z. Dong, Z. Gong, B. Chen, T. Sheng, Y. Cao, Q. He, P. Zhao and Y. Jiang, *IEEE Sens. J.*, 2023, **23**, 29494–29501.
95 J. Lin, J. Li, W. Li, S. Chen, Y. Lu, L. Ma, X. He and Q. Zhao, *Composites, Part A*, 2024, **178**, 108003.

96 J. Luo, N. Ji, W. Zhang, P. Ge, Y. Liu, J. Sun, J. Wang, Q. Zhuo, C. Qin and L. Dai, *Mater. Horiz.*, 2022, **9**, 1503–1512.
97 Z. Dong, D. Shen, Z. Gong, D. Zhang and Y. Jiang, *IEEE Sens. J.*, 2022, **22**, 15884–15892.
98 N. T. Nguyen, *Flow Meas. Instrum.*, 1997, **8**, 7–16.
99 J. Chen, K. Zhang, L. Wang and M. Yang, *Sensors*, 2020, **20**, 4804.
100 S. A. Araujo-Estrada, F. Salama, C. M. Greatwood, K. T. Wood, T. S. Richardson and S. P. Windsor, in *AIAA Guidance, Navigation, and Control Conference*, American Institute of Aeronautics and Astronautics, 2017, DOI: 10.2514/6.2017-148710.2514/6.
101 A. C. Hollenbeck, R. Grandhi, J. H. Hansen and A. M. Pankonien, *AIAA J.*, 2024, **62**, 3803–3812.
102 R.-H. Ma, C.-Y. Lee, Y.-H. Wang and H.-J. Chen, *Microsyst. Technol.*, 2008, **14**, 971–977.
103 R.-H. Ma, Y.-H. Wang and C.-Y. Lee, *Sensors*, 2011, **11**, 2715–2727.
104 P. Mohindru, *Heat and Mass Transfer*, 2023, **59**, 2149–2166.